ISSN: 1692-7257 - Volume 1 – Number 47 – 2026

RCTA
Revista Colombiana de Tecnologías de Avanzada
UNIPAMPLONA

Digital Object Identifier: 10.24054/rcta.v1i47.4283

Comparison of color normalization techniques for reduction of tissue heterogeneity in breast cancer histopathological images

Evaluación de técnicas de normalización de color para reducción de heterogeneidad de tejidos en imágenes histopatológicas de cáncer de mama

MSc (c). Diego Andrés Castellano Carvajal[1], PhD. Sergio Alexander Castro Casadiego[2], MSc. Carlos Vicente Niño Rondón[2], PhD. Byron Medina Delgado[2]

*[1] **Pontificia Universidad Javeriana,** Faculty of Engineering and Sciences, Cali, Valle del Cauca, Colombia.*
*[2] **Universidad Francisco de Paula Santander,** Department of Electrical and Electronic Engineering, Cúcuta, Norte de Santander, Colombia.*

***Correspondence:** diegocastellano@javerianacali.edu.co*

***Received:** July 01, 2025. **Accepted:** December 20, 2025. **Published:** January 01, 2026.*

***How to cite:** D. A. Castellano Carvajal, S. A. Castro Casadiego, C. V. Niño Rondón y B. Medina Delgado, "Comparison of color normalization techniques for reduction of tissue heterogeneity in breast cancer histopathological images", RCTA, vol. 1, n.º. 47, pp. 26-33, Jan. 2026.*
Recuperado de https://ojs.unipamplona.edu.co/index.php/rcta/article/view/4283

Abstract: Color normalization in histopathological images is considered an initial step aimed at contributing to consistency in the computational analysis of hematoxylin and eosin (H&E)-stained tissues. In this work, three color normalization methods are evaluated in histopathological images of breast cancer (Macenko, Reinhard, and Vahadane) using quantitative metrics ORB, SSIM, and histogram correlation. In terms of ORB and SSIM, Vahadane stood out for better preserving morphological structures with consistently high values, which is crucial for computational analysis. Nevertheless, Vahadane presented variability in histogram correlation, in contrast to Macenko and Reinhard, who achieved higher and consistent correlations across all samples with average values of 0.9628 and 0.9385. This highlights that the choice of method depends on the balance between structural fidelity and chromatic distribution depending on the case.

Keywords: Color normalization, histopathologic imaging, breast cancer.

Resumen: La normalización del color en imágenes histopatológicas se considera una etapa inicial orientada para contribuir con la coherencia en el análisis computacional de tejidos teñidos con hematoxilina y eosina (H&E). En este trabajo, se evalúan tres métodos de normalización de color en imágenes histopatológicas de cáncer de mama (Macenko, Reinhard y Vahadane) utilizando métricas cuantitativas ORB, SSIM y correlación de histogramas. En términos de ORB y SSIM, Vahadane destacó por preservar mejor las estructuras morfológicas con valores consistentemente altos, lo que es crucial para análisis computacional. No obstante, Vahadane presentó variabilidad en la correlación de histogramas, en contraste con Macenko y Reinhard, quienes lograron correlaciones más altas y consistentes en todas las muestras con valores promedio de 0.9628 y 0.9385. Esto

resalta que la elección del método depende del balance entre fidelidad estructural y distribución cromática según el caso.

Palabras clave: Normalización de color, imágenes histopatológicas, cáncer de mama.

1. INTRODUCTION

In recent years, breast cancer has become one of the leading causes of death among women worldwide. [1]. There has been a significant increase in the incidence of new cases, surpassing even lung cancer as the most common type of cancer in the world. In this context, the sentinel lymph node plays a crucial role, as it represents the first point of metastasis in the lymph nodes associated with breast cancer. This node receives the line from the primary tumor, facilitating the spread of cancer cells [2].

Histopathological images stained with hematoxylin and eosin (H&E) refer to an important tool in the diagnosis of breast cancer. However, these images present variability in staining caused by differences in reagents and image acquisition conditions that can generate heterogeneity in tissues, affecting computational analysis processes and interpretation by pathologists [3].

Various color normalization techniques have been developed to standardize the chromatic appearance of images and facilitate their comparison, improving the performance of segmentation models [4] and automated classification [5]. Among the most widely used techniques are the Macenko, Reinhard and Vahadane methods, which apply different mathematical approaches to adjust the color distribution in images [6].

de Haan et al. [7] present an innovative deep learning-based framework to transform H&E-stained tissue images into special stains such as Masson's Trichrome, PAS and Jones silver stain. This method uses spatially registered data to train supervised deep neural networks, eliminating the reliance on unpaired data. Generating special stains (PAS, Masson's Trichrome and Jones) from H&E images improved the diagnosis of several non-neoplastic renal diseases by 22.4 %.

Runz et al. [8] investigate the use of CycleGAN (cyclic generative adversarial network) for color normalization in hematoxylin-eosin (H&E) stained histological images with the aim of reducing variations caused by differences in image acquisition, tissue processing and staining. Structural Similarity Index Measure (SSIM) scores indicated high similarity between the real images and their reconstructions, with scores above 0.9 for both imaging domains.

Zhao et al. [9] present RestainNet, a self-supervised learning model designed to digitally normalize color spots in pathological images, is proposed. This innovative model utilizes a digital re-coloring process of grayscale images, applying digital Hematoxylin (H) and Eosin (E) dyes extracted using the Beer-Lambert Law. In addition, a novel staining loss function is introduced to ensure the correction of dye intensity during the re-staining process. Quantitative comparisons with other methods demonstrated that RestainNet outperforms existing approaches on several metrics. RestainNet scored 0.917 ± 0.019 on the FSIM (Feature Similarity Index), which is higher than other methods. Moreover, on the PSNR (Peak Signal-to-Noise Ratio) RestainNet achieved 21.550 ± 3.665, showing significant improvement.

Franchet et al. [10] present two new techniques, AugmentHE and HEnorm, are presented, which seek to mitigate bias in the classification of histological images. These techniques improve the accuracy and generalization of machine learning models used in digital pathology, specifically in the histological grading of breast cancer. When combining the PACS05 and PACS08 datasets, the combination of HEnorm and augHE showed an AUC of 0.85 ± 0.02, compared to 0.82 ± 0.02 in PACS05 and 0.73 ± 0.07 in PACS08 separately.

The method proposed by Tosta et al. [11], called SCN-RDL, focuses on estimating color appearance matrices and density maps of stains. Approaches for pixel selection and weight definition are introduced, thus improving color estimation. The proposed normalization was evaluated using the DCIS-UDH and UCSB databases. The results showed that the SCN-RDL color normalization method is effective in improving the quality and consistency of hematoxylin and eosin (H&E) stained images, reaching a FSIM (Feature Similarity Index) of 0.9866.

Jeong et al. [12] develop a score-based diffusion model for stain normalization. To avoid confusion in color transfer, they propose a stain separation

method using sparse non-negative matrix factorization (SNMF) and overlapping moving windows to avoid grid artifacts. The proposed method outperformed conventional and generative adversarial network-based methods on several quantitative merits, showing robustness on unseen data.

Tabatabaei et al. [13] propose a content-based histopathological image retrieval (CBHIR) framework that uses color normalization to improve cancer diagnosis accuracy. Macenko, Vahadane and BKSVD techniques were evaluated on the CAMELYON17 dataset, with BKSVD standing out as the most effective, achieving a 97 % improvement in image retrieval accuracy. The work demonstrates that effective color normalization reduces variability, enhancing critical features in images and optimizing the performance of computer-assisted tools.

This paper presents the evaluation and comparison of these three-color normalization techniques in histopathological images of lymph nodes with breast cancer. The evaluation is performed using criteria that measure the preservation of structural and textural characteristics, as well as the classification of histograms, which allows the analysis of the chromatic similarity between normalized images.

2. METHODOLOGY

A three-stage methodology is proposed. In the first stage, the nature of the CAMELYON dataset is analyzed. In the second stage, color normalization methods are applied to histopathological images. Finally, in the third stage, the efficiency of color normalization methods on histopathological images is compared.

2.1. Nature of the CAMELYON dataset

CAMELYON refers to the dataset focused on the detection of breast cancer metastases in lymph nodes that contain Whole Slide Images (WSI) of hematoxylin and eosin (H&E) stained tissues obtained from patient lymph node samples. The images are digitized using high-resolution slide scanners to perform deep analysis at the cellular level. For this work, the CAMELYON16 version was used, which contains 400 WSIs images. They use color depth with red, green, and blue channels, and are stored in TIFF (Tagged Image File Format) format [14].

The dataset highlights the variation in the staining of the images, produced by the differences in the H&E staining processes, the quality of reagents and parameters in the digitalization, presenting a challenge in the automated analysis that affects the performance of the segmentation models [15]. Therefore, the CAMELYON dataset is suitable for comparing and evaluating color normalization techniques in terms of standardizing the appearance of images and reducing the influence of variations. Table 1 presents a summary of the dataset, including technical and descriptive aspects of the histopathology images.

Table 1. *Technical summary of the CAMELYON16 dataset*

Aspect	Detail
Data type	Digitalized histopathological images
Source	Lymph nodes from patients with breast cancer
Resolution	40x (high resolution)
Image format	.tiff (lossless format)
Image size	Approximately 100,000 x 100,000 pixels
Color depth	24 bits (RGB)
Number of slides	400
Staining technique	Hematoxylin and eosin (H&E)

Source: *Own elaboration*

2.2. Techniques for color normalization

For analysis and comparison of color normalization methods, a preprocessing for patch extraction was applied, where each WSI was divided into patches of size 1024x1024 with a focus on regions with relevant tissue and variations in H&E staining.

2.2.1. Macenko

This method proposed by Macenko [16] is based on the separation of H&E stains using an optical model and normalization of color intensities. Images are converted from RGB color space to optical color space using the Beer-Lambert model to separate staining components as shown in equation (1), where I is the normalized RGB vector.

$$OD = -\log_{10}(I) \quad (1)$$

Singular value decomposition is applied on the color intensity matrix to estimate the stain vectors representing the predominant color directions in the image as presented in equation (2), where OD is the optical density value observed and V and S are the matrices of the stain vectors and the saturations of each of the stains, respectively.

$$S = V^{-1}OD \quad (2)$$

The color intensities of the source image are projected onto the staining vectors, and the staining intensities are normalized with a linear transformation fitted with the mean and standard deviation of the staining intensities. Finally, the image is reconstructed in RGB space using the normalized intensities and staining vectors.

2.2.2. Reinhard

The Reinhard method [17] was implemented to normalize H&E images, where the color distribution of the target image is transferred to the source image in CIE Lab color space. Initially, the images are converted from RGB to CIE Lab. Then, the means and standard deviations of the l, α, and β channels are calculated for the images. Subsequently, a linear transformation is applied on the pixels of the source image using the means and standard deviations of the reference image as shown in equations (3), (4), and (5). Finally, the normalized image is converted to RGB space.

$$l' = \frac{\sigma_{l,source}}{\sigma_{l,target}}\left(l - \langle l\rangle_{target}\right) + \langle l\rangle_{source} \quad (3)$$

$$\alpha' = \frac{\sigma_{\alpha,source}}{\sigma_{\alpha,target}}\left(\alpha - \langle \alpha\rangle_{target}\right) + \langle \alpha\rangle_{source} \quad (4)$$

$$\beta' = \frac{\sigma_{\beta,source}}{\sigma_{\beta,target}}\left(\beta - \langle \beta\rangle_{target}\right) + \langle \beta\rangle_{source} \quad (5)$$

2.2.3. Vahadane

The method proposed by Vahadane [18] was implemented, which is based on the separation of hematoxylin and eosin (H&E) stains using an optical model and normalized image reconstruction. Initially, RGB images are converted to optical density OD space to linearize the relationship between light intensity and stain concentration, allowing for more effective stain separation. Next, a non-negative matrix factorization with sparsity constraints (SNMF) is used to separate stain spots as shown in equation (6), where V is the optical density matrix, W contains the color vectors of the spots, and H the density maps.

$$V = WH \quad (6)$$

The staining concentration matrix is estimated by minimizing a cost function to avoid non-negativity and concentration spread as seen in equation (7), subject to $W,\ H \geq 0$, where λ is the parameter controlling the spread of the intensity maps H.

$$\min_{W,H} \frac{1}{2}\|V - WH\|_F^2 + \lambda \sum_{j=1}^{r} \|H(j,:)\|_1 \quad (7)$$

Dye concentrations from the source image are normalized with a linear transformation in concentration space to match the mean and standard variance of dye concentrations from the target image. The normalized image is reconstructed in RGB space using the normalized concentrations and dye matrix from the reference image to preserve tissue structures with a standardized color distribution as given in equation (8), where $V_{norm} = W_t H_s^{norm}$, W_t is the color vector matrix of the target image, and H_{norm}^S is the normalized density map matrix of the source image.

$$I_{norm} = I_o \exp\left(-V_{norm}\right) \quad (8)$$

2.3. Evaluation criteria

ORB (Oriented Fast and Rotated Brief) is a detection algorithm and descriptor used to compare features between histopathological images before and after normalization, to evaluate the normalized image in terms of preservation of tissue and cellular structures. ORB combines two main components: FAST (Features from Accelerated Segment Test), a point detector to identify image regions of interest based on pixel intensities, and BRIEF (Binary Robust Independent Elementary Features), a descriptor used to represent the detected features.

Structural Similarity Index (SSIM) is an image similarity metric based on luminance, contrast, and structural components, which considers human visual perception to evaluate the quality of medical images and quantify the structural similarity between the original and normalized images. Equation (9) describes the metric, where μ_x and μ_y are the means of images x and y, σ_x^2 and σ_y^2 are the variances of images x and y, σ_{xy} is the covariance between x and y, and C_1 and C_2 are the constants that avoid division by zero.

$$SSIM\ (x,y) = \frac{(2\mu_x\mu_y + C_1)(2\sigma_{xy} + C_2)}{(\mu_x^2 + \mu_y^2 + C_1)(\sigma_x^2 + \sigma_y^2 + C_2)} \quad (9)$$

The statistical correlation method was also used to analyze the distribution histograms generated by each greyscale image. In this case, H1, H2, H3 and H4 represent the histograms corresponding to the original image, the image normalized by the Macenko method, the image resulting from the Reinhard method and the image obtained with the Vahadane method, respectively. These histograms

were normalized in the same scale space to facilitate the comparison of the similarity between the images.

Correlation was applied with descriptive statistics (mean, standard deviation, minimum and maximum) to determine the relationship between the histograms, obtaining values in the range of -1 to 1. A value close to 1 indicates a perfect direct correlation, while a value close to -1 suggests a perfect inverse correlation. On the other hand, a value close to 0 implies that there is no correlation between the variables. Equation (10) describes the methodology used to calculate the point-to-point correlation from the values obtained in the histograms.

$$d(H_1, H_{2,3,4}) = \frac{\Sigma_I (H_1(I) - \bar{H}_1)(\bar{H}_{2,3,4}(I) - \bar{H}_{2,3,4})}{\sqrt{\Sigma_I (H_1(I) - \bar{H}_1)^2 * \Sigma_I (H_{2,3,4}(I) - \bar{H}_{2,3,4})^2}} \quad (9)$$

3. RESULTS AND DISCUSSION

Based on the proposed methodology, Fig. 1 presents the preprocessing performed on the images of the CAMELYON16 dataset resized to 1024x1024 pixels, where section A shows the images in RGB representation, section B shows the target image that is representative of the dataset and captures the typical staining characteristics (hematoxylin and eosin intensity). Section C shows the Macenko normalization, in D the Reinhard normalization, and in E the Vahadane normalization.

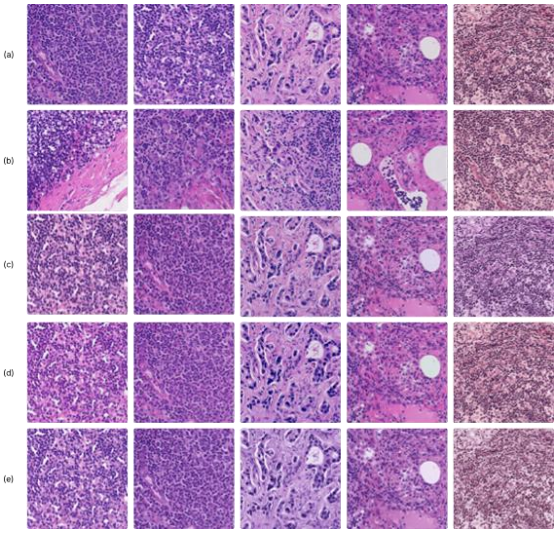

***Fig. 1**. Color normalization of CAMELYON16 H&E images*
***Source:** own elaboration*

Likewise, Fig. 2 shows the histograms obtained in each of the five test images for the validation of the H&E image color normalization methods, where the redistribution of the color channels and the variations between the histograms that represent the adjustments suggested by each model based on the sensitivity to differences in staining or illumination can be seen.

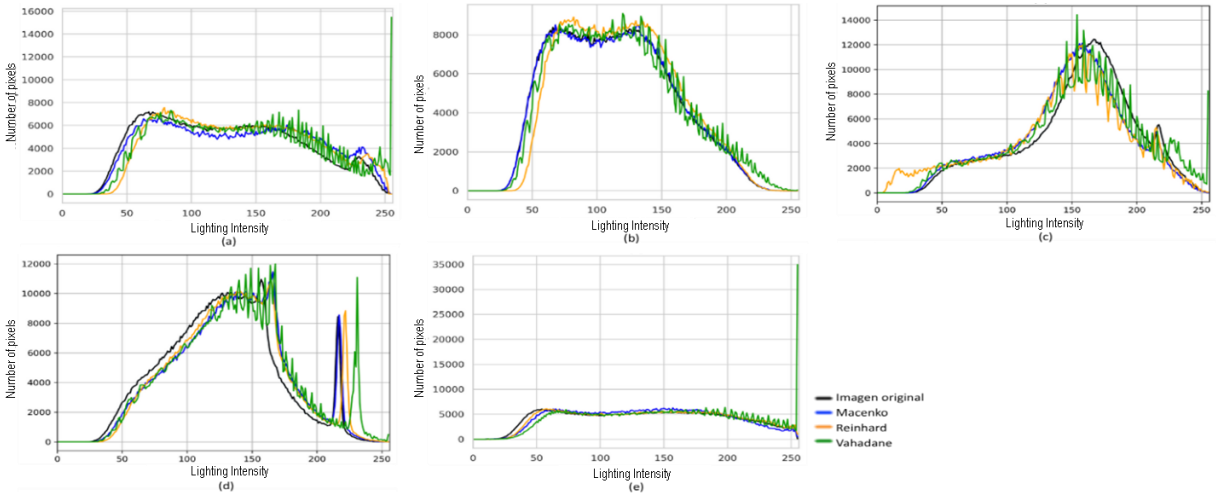

***Fig. 2**. Histogram obtained for the sample images*
***Source:** own elaboration*

The histograms corresponding to A, B, and E showed better consistency in the distribution of intensities after normalization. This was reflected in a more uniform distribution of intensity values, with well-defined peaks and less dispersion in the color channels (hematoxylin and eosin). In contrast, histograms C and D showed greater variability in the distribution of intensities. This could be due to inherent differences in the original staining of these images, such as excessive or insufficient staining, or

the presence of artifacts that made normalization difficult.

Table 2 presents the correlation values and descriptive statistics between three histopathological image normalization methods Macenko, Reinhard and Vahadane. Five samples representing histopathological images from different patients or tissues were evaluated. It is observed that in Sample 1, Macenko and Reinhard have a high correlation of 0.9540 and 0.9038, respectively, while Vahadane has a lower correlation with a value of 0.8213. On the other hand, in Sample 5, Vahadane shows a significantly lower correlation compared to Macenko and Reinhard. It is noted that Macenko and Reinhard show consistently high correlation values across all samples, suggesting that these methods produce similar results in color normalization. Vahadane, although a more advanced method, shows a more variable correlation. In particular, in Sample 5, the correlation is significantly lower, which might indicate that this method does not fit well to certain types of images or tissues [19]. The variability in correlation values suggests that the choice of normalization method may depend on the tissue type or specific image characteristics. In terms of descriptive statistics, Macenko has the highest mean with a value of 0.9628 and the lowest standard deviation with 0.0189, indicating that it is the most consistent and reliable method in terms of correlation. Reinhard also shows a high mean (0.9385) and a moderate standard deviation (0.0316), suggesting that it is a robust method [20], although slightly less consistent than Macenko. Vahadane has the lowest mean with 0.8281 and the highest standard deviation (0.1811), demonstrating a higher variability in its performance. This suggests that although it may perform very well in some cases (e.g. in Sample 2), in other cases its performance is significantly lower (e.g. in Sample 5).

Table 2. *Correlation values and descriptive statistics by normalization method*

Sample	Macenko	Reinhard	Vahadane	Statistics	Macenko	Reinhard	Vahadane
Sample 1	0.9540	0.9038	0.8213	**Mean**	0.9628	0.9385	0.8281
Sample 2	0.9994	0.9677	0.9851	**Standard deviation**	0.0189	0.0316	0.1811
Sample 3	0.9549	0.9223	0.9359	**Minimum**	0.9508	0.9038	0.5130
Sample 4	0.9508	0.9197	0.8853	**Maximum**	0.9994	0.9791	0.9851
Sample 5	0.9547	0.9791	0.5130				

Source: *Own elaboration*

Likewise, Fig. 3 shows the box plots to compare the distributions of the normalization methods on the ORB and SSIM metrics. For the ORB analysis, the Macenko method produces high values in some areas and tends to generate a less uniform color distribution (high dispersion).

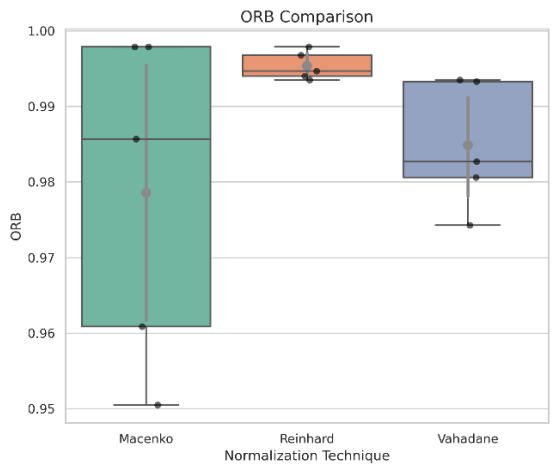

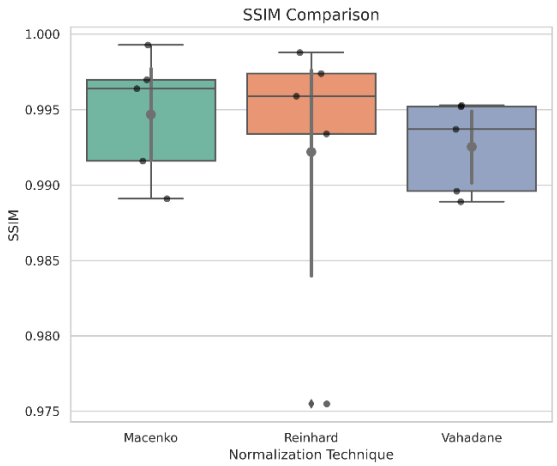

Fig. 3*. Boxplot of ORB and SSIM metrics*
Source: *own elaboration*

The median is slightly lower than the other techniques and the intensity values are lower, affecting the visual interpretation of the normalized images. In addition, its performance is less stable and consistent. Reinhard shows a slightly higher median than Macenko and his values are more

grouped, indicating greater stability in the results. Vahadane also presents a slightly high median and has less dispersion than Macenko, showing greater consistency. On the other hand, in the SSIM analysis, Macenko presents a high median, which indicates that in most cases the normalized images are similar to the reference image.

In addition, it presents low dispersion and does not present significant variations between the images, showing greater consistency. Reinhard showed a higher dispersion and the normalized images vary more widely, due to its sensitivity to differences in images and dependence on statistical color values. The method is not as consistent as Macenko and its performance can be acceptable for some images, but less effective for others. In general, the normalization quality with Reinhard is acceptable and does not exceed that of Macenko. On the other hand, Vahadane has a median close to Macenko and its dispersion is low, indicating stability between values.

4. CONCLUSIONS

Three color normalization techniques, Macenko, Reinhard, and Vahadane, were compared on hematoxylin and eosin (H&E)-stained histopathological images of breast cancer lymph nodes. For the evaluation, histogram correlation and ORB and SSIM similarity metrics were used, which allow measuring the consistency in color distribution and structural similarity between normalized images and their original versions. The results obtained indicate that Vahadane is the technique with the best overall performance, since it presented higher values and lower variability in ORB and SSIM, suggesting greater stability and fidelity in the preservation of tissue morphological features, which is crucial for computational analysis applications, such as automated segmentation and classification, where the preservation of cellular and tissue structures contributes to the accuracy of the model. However, the results of the histogram correlation showed that Vahadane presents significantly lower values compared to Macenko and Reinhard. While the technique better preserves the structure and texture patterns of the images, it modifies the tones and colour distribution more, generating images with more significant chromatic differences compared to the original. In contrast, Macenko and Reinhard preserve greater similarity in colour distribution, but with a slight loss in structural preservation. The comparison provides information to improve standardisation in the processing of histopathological images, which can positively impact computer-assisted diagnosis and the development of artificial intelligence models applied to digital pathology.

REFERENCES

[1] C. Kaushal, S. Bhat, D. Koundal, and A. Singla, “Recent Trends in Computer Assisted Diagnosis (CAD) System for Breast Cancer Diagnosis Using Histopathological Images,” *IRBM*, vol. 40, no. 4, pp. 211–227, Aug. 2019, doi: 10.1016/j.irbm.2019.06.001.

[2] S. yang Tang, L. Li, Y. lin Li, A. yuan Liu, M. jun Yu, and Y. ping Wan, “Distribution and location of Daxx in cervical epithelial cells with high risk human papillomavirus positive,” *Diagn Pathol*, vol. 9, no. 1, Jan. 2014, doi: 10.1186/1746-1596-9-1.

[3] F. Li, J. Ma, T. Wen, Z. Tian, and H. N. Liang, “HI-Net: A novel histopathologic image segmentation model for metastatic breast cancer via lightweight dataset construction,” *Heliyon*, vol. 10, no. 19, p. e38410, Oct. 2024, doi: 10.1016/J.HELIYON.2024.E38410.

[4] A. Agrawal and V. Maan, “Enhanced Brain Tumor Segmentation and Size Estimation in MRI Samples using Hybrid Optimization,” *Data and Metadata*, vol. 3, pp. 408–408, Jan. 2024, doi: 10.56294/DM2024408.

[5] G. A. Ansari, S. S. Bhat, M. D. Ansari, S. Ahmad, and H. A. M. Abdeljaber, “Prediction and Diagnosis of Breast Cancer using Machine Learning Techniques,” *Data and Metadata*, vol. 3, p. .346-.346, Sep. 2024, doi: 10.56294/DM2024.346.

[6] T. A. Azevedo Tosta, P. R. de Faria, L. A. Neves, and M. Z. do Nascimento, “Computational normalization of H&E-stained histological images: Progress, challenges and future potential,” *Artif Intell Med*, vol. 95, pp. 118–132, Apr. 2019, doi: 10.1016/J.ARTMED.2018.10.004.

[7] K. de Haan *et al.*, “Deep learning-based transformation of H&E stained tissues into special stains,” *Nat Commun*, vol. 12, no. 1, Dec. 2021, doi: 10.1038/s41467-021-25221-2.

[8] M. Runz, D. Rusche, S. Schmidt, M. R. Weihrauch, J. Hesser, and C. A. Weis, “Normalization of HE-stained histological images using cycle consistent generative adversarial networks,” *Diagn Pathol*, vol. 16, no. 1, Dec. 2021, doi: 10.1186/s13000-021-01126-y.

[9] B. Zhao *et al.*, “RestainNet: A self-supervised digital re-stainer for stain normalization,” *Computers and Electrical Engineering*, vol. 103, Oct. 2022, doi: 10.1016/j.compeleceng.2022.108304.

[10] C. Franchet *et al.*, “Bias reduction using combined stain normalization and augmentation for AI-based classification of histological images,” *Comput Biol Med*, vol. 171, Mar. 2024, doi: 10.1016/j.compbiomed.2024.108130.

[11] T. A. A. Tosta, A. D. Freitas, P. R. de Faria, L. A. Neves, A. S. Martins, and M. Z. do Nascimento, “A stain color normalization with robust dictionary learning for breast cancer histological images

processing," *Biomed Signal Process Control*, vol. 85, Aug. 2023, doi: 10.1016/j.bspc.2023.104978.

[12] J. Jeong, K. D. Kim, Y. Nam, C. E. Cho, H. Go, and N. Kim, "Stain normalization using score-based diffusion model through stain separation and overlapped moving window patch strategies," *Comput Biol Med*, vol. 152, Jan. 2023, doi: 10.1016/j.compbiomed.2022.106335.

[13] Z. Tabatabaei, F. Pérez Bueno, A. Colomer, J. O. Moll, R. Molina, and V. Naranjo, "Advancing Content-Based Histopathological Image Retrieval Pre-Processing: A Comparative Analysis of the Effects of Color Normalization Techniques," *Applied Sciences (Switzerland)*, vol. 14, no. 5, Mar. 2024, doi: 10.3390/app14052063.

[14] E. Bütün, M. Uçan, and M. Kaya, "Automatic detection of cancer metastasis in lymph node using deep learning," *Biomed Signal Process Control*, vol. 82, p. 104564, Apr. 2023, doi: 10.1016/J.BSPC.2022.104564.

[15] M. Veta, P. J. van Diest, R. Kornegoor, A. Huisman, M. A. Viergever, and J. P. W. Pluim, "Automatic Nuclei Segmentation in H&E Stained Breast Cancer Histopathology Images," *PLoS One*, vol. 8, no. 7, p. e70221, Jul. 2013, doi: 10.1371/JOURNAL.PONE.0070221.

[16] M. Macenko *et al.*, "A method for normalizing histology slides for quantitative analysis," *Proceedings - 2009 IEEE International Symposium on Biomedical Imaging: From Nano to Macro, ISBI 2009*, pp. 1107–1110, 2009, doi: 10.1109/ISBI.2009.5193250.

[17] E. Reinhard, M. Ashikhmin, B. Gooch, and P. Shirley, "Color transfer between images," *IEEE Comput Graph Appl*, vol. 21, no. 5, pp. 34–41, Sep. 2001, doi: 10.1109/38.946629.

[18] A. Vahadane *et al.*, "Structure-Preserving Color Normalization and Sparse Stain Separation for Histological Images," *IEEE Trans Med Imaging*, vol. 35, no. 8, pp. 1962–1971, Aug. 2016, doi: 10.1109/TMI.2016.2529665.

[19] A. Sethi *et al.*, "Empirical comparison of color normalization methods for epithelial-stromal classification in H and E images," *J Pathol Inform*, vol. 7, no. 1, p. 17, Jan. 2016, doi: 10.4103/2153-3539.179984.

[20] S. Roy, S. Panda, and M. Jangid, "Modified Reinhard Algorithm for Color Normalization of Colorectal Cancer Histopathology Images," *2021 29th European Signal Processing Conference (EUSIPCO)*, pp. 1231–1235, Aug. 2021, doi: 10.23919/EUSIPCO54536.2021.9616117.